2023-01-1615 Published 31 Oct 2023

Engine Operating Conditions, Fuel Property Effects, and Associated Fuel–Wall Interaction Dependencies of Stochastic Preignition

Derek Splitter, Vicente Boronat Colomer, Sneha Neupane, and William Partridge Oak Ridge National Laboratory

Citation: Splitter, D., Boronat Colomer, V., Neupane, S., and Partridge, W., "Engine Operating Conditions, Fuel Property Effects, and Associated Fuel–Wall Interaction Dependencies of Stochastic Preignition," *SAE Int. J. Advances & Curr. Prac. in Mobility* 6(5):2422-2441, 2024, doi:10.4271/2023-01-1615.

This article was presented at the Energy & Propulsion Conference & Exhibition, November 7-9, 2023.

Received: 16 Jun 2023 Revised: 26 Jul 2023 Accepted: 1 Aug 2023

Abstract

This work for the Coordinating Research Council (CRC) explores dependencies on the opportunity for fuel to impinge on internal engine surfaces (i.e., fuel–wall impingement) as a function of fuel properties and engine operating conditions and correlates these data with measurements of stochastic preignition (SPI) propensity. SPI rates are directly coupled with laser–induced florescence measurements of dye-doped fuel dilution measurements of the engine lubricant, which provides a surrogate for fuel–wall impingement. Literature suggests that SPI may have several dependencies, one being fuel–wall impingement. However, it remains unknown if fuel-wall impingement is a fundamental predictor and source of SPI or is simply a causational factor of SPI. In this study, these relationships on SPI and fuel-wall impingement are explored using 4 fuels at 8 operating conditions per fuel, for 32 total test points. The fuels were directly injected at two different injection timings: an earlier injection timing that initially targets the piston crown and a later injection timing that targets the cylinder liner. At each injection timing, the engine was operated at both 90°C and 70°C coolant and lubricant temperatures, and 185 and 200 kPa absolute intake manifold pressure. This work serves as an exploratory effort to down select conditions and provide initial fuel properties of interest for a secondary study to explore fuel property specific effects on fuel-wall interaction and SPI propensity.

Significant findings from this initial operating condition and fuel property exploratory work are: 1. reduced engine operating coolant and lubricant temperatures, along with 2. retarded injection timings were required to increase SPI propensity. Moreover, at these conditions some fuel specific effects were also observed; specifically, increased ethanol content increased measured dye–wall (i.e., fuel–wall) interaction. However, despite increased dye–wall interaction, the increased volatility of the ethanol containing fuels also reduced the estimated fuel retention in the top-ring zone and associated measured SPI propensity. Thus, the findings of this unique approach to explore relationships between fuel-wall impingement and SPI highlight that SPI propensity is more directly proportional to retained fuel, and not simply fuel–wall impingement. Fuel retention was found to be directly influenced by complex fuel property and engine operating condition relationships. Either retarded injection timings and/or increased fuel volatility increased fuel wall-impingement, while less volatile fuels and/or reduced coolant temperatures increased fuel retention. Therefore, for a given operating condition, the data highlights that greater volatile fuels exhibit increased fuel wall impingement without increased fuel retention or SPI propensity, while less volatile fuels could exhibit reduced fuel-wall impingement but increased fuel retention and SPI propensity rates.

Introduction

Stochastic preignition (SPI) is an abnormal combustion process that initiates combustion prior to spark discharge in boosted spark ignition (SI) engines. SPI can be a precedent of severe knock events (super or mega knock), presenting a limitation on downsizing [1]. This unwanted SPI phenomenon can result in catastrophic engine failure and is a significant contributor to in-field warranty claims for automotive manufacturers [2].

SPI has been researched for more than a decade, but the fundamentals remain unclear [2, 3, 4, 5, 6, 7, 8, 9]. Chapman et al. [10] performed a review of abnormal ignition in gasoline engines, especially preignition, which has been investigated since the early 1920s. More recently, research has covered

several areas focusing on the effects of mixture and lubricant properties that seem to cause higher SPI occurrence [11, 12]. Within that context, SPI has been shown to be heavily influenced by operating conditions, and by fuel and lubricant properties [13, 14, 15, 16, 17, 18, 19, 20, 21]. Thus, studying SPI is challenging, and therefore, the research community has also investigated different approaches to assess SPI [22].

Among others, theories on particulate matter or deposits and the opportunity for fuel to impinge on internal engine surfaces (i.e., fuel–wall impingement) have emerged as the most prominent theories on fundamental causes of SPI. With respect to the particulate matter theory, literature suggests a correlation between the particulate matter index (PMI) and the 50% fuel distillation point (T50) and SPI activity [22]. However, it is not clear whether this is purely a distillation effect or if SPI is correlated with fuel composition. Others using high polyaromatic fuel, found a correlation between SPI activity and increased particulate mass and particle number, and that blooms of smoke were observed when SPI events occurred [20]. However, the study was unable to identify whether soot was a cause of SPI or a result of SPI.

Particulate matter index (PMI) is an effective parameter that links fuel properties to the particle matter emissions for gasoline-like fuels, [23]. Additionally, Aikawa et al. [23] concluded that high–boiling point aromatic components typically containing high–double bond equivalent values are prone to increase the particle number emissions. Thus, a first theory is that PMI might act as an aromatic content indicator of fuel and thereby serve as a predictor of SPI activity. Recent work by Boronat et al. [24] provides further evidence to understand whether fuel PMI is a fundamental driver for SPI. Specifically, that work highlighted that PMI has more of an indicator role for SPI to occur from fuel properties than particulate matter formed from increased PMI fuels itself.

The second and potentially more prevalent theory on SPI generation is fuel–wall impingement [22]. In this framework, SPI is suspected to result from fuel retention and interaction in the top ring zone (TRZ) of the engine. At high load conditions, high fueling rates deliver a large fuel mass and penetration into the combustion chamber, increasing the opportunity for fuel to impinge on internal engine surfaces, specifically the cylinder liner wall. If the impinged fuel is not evaporated off the internal surfaces, the impinged fuel may mix with lubricant and combustion residues at the TRZ. The resultant liquid, if accumulated in sufficient quantities, can be ejected into the combustion chamber, where expelled droplets become uncontrolled ignition sources [25, 26, 27].

The liquid composition of such droplets is unknown, but the liquid is likely more reactive than gasoline and easier to ignite than oil as the lubricant at TRZ suffers more aggressive oxidation and degradation than at the sump oil [28, 29, 30, 31]. Moreover, Splitter et al. showed that under elevated loads, the TRZ liquid composition is primarily composed of the heavier species in the fuel [32] and also evolves through oxidation and nitration processes as shown by Kim et al. [33] and Lee et al. [34].

The evolving TRZ liquid also has the potential to interact with the lubricant and its associated antioxidants, detergents, and anti-wear packages, generating a unique liquid phase chemistry at the TRZ. Others suggest that calcium components used in the detergent packages can promote SPI regardless of the type of calcium component [17], highlighting that lubricant additives interacting with impinged fuel may be a significant factor that affects SPI propensity [11, 35].

Dahnz et al. [36] conducted an experimental campaign considering causes of SPI. Furthermore, using a UV-sensitive high-speed camera to optically measure the evolution of SPI onset and progression in the combustion chamber, they concluded the most relevant factor of SPI is oil dilution caused by fuel–spray impingement that directly effects the droplets released. However, despite the fact that fuel-in-oil dilution has been considered one of the most relevant underlying mechanisms of SPI, very few public disclosures have been made because of the difficulties of such investigations.

Current gasoline direct injection engines are prone to suffer from wall-wetting because the fuel is delivered inside the cylinder during the intake stroke [5]. Recently, Splitter et al. [37, 38] deployed a laser-induced fluorescence diagnostic highlighted by Neupane et al. [39] in the engine lubricant to measure fuel–wall impingement as a function of load and start of injection (SOI) timing in a modern gasoline direct injection engine. The approach was based on a previous study by Parks et al. [40]. The findings of Splitter et al. [37, 38] highlighted with direct measurements that at high loads and or at retarded SOI timings, fuel–wall impingement can become exacerbated. Additionally, Splitter et al. [37] suggested that the preferential vaporization of the fuel species may play a key role regarding the TRZ liquid composition.

Based on historical and recent findings on SPI fundamentals, the present work is focused on understanding the role of fuel–wall interaction on SPI, and specifically if fuel–wall interaction results in increased SPI rates. To improve this understanding, we used a dedicated experimental campaign at 2,000 rpm engine speed with two SOI timings at SPI-prone operating conditions, two coolant temperatures, and two loads. The more advanced 310°CA before top dead center firing ($bTDC_f$) SOI timing was used to examine more smoke-prone conditions [41], and a 220°CA $bTDC_f$ SOI timing was used to target the cylinder liner and focus on the effect of fuel impingement on SPI activity [37]. Four fuels with different distillation curves, composition, and PMIs were tested. A laser-induced fluorescence optical diagnostic tool was coupled to a single-cylinder engine (SCE) to measure the oil dilution at all tested conditions. This work provides novel insights on fuel spray-wall interactions and associated fuel retention that influence SPI with a variety of fuel properties. Results were analyzed to elaborate on fuel spray–wall interaction and general fuel effects that fundamentally affect SPI propensity. This Phase 1 work within the AVFL-33 project will highlight operating conditions and factors affecting SPI, where a more detailed follow-on Phase 2 project will explore fuel-specific chemistries and properties that affect SPI propensity.

Methods

Fuel in Lube Diagnostic

The laser-induced fluorescence optical diagnostic tool developed by Neupane et al. [39, 42] was employed in the present work to evaluate the effect of fuel–wall interactions at SPI-prone conditions. The fuel in lube (FiL) instrument

measured dye (Model TP-3400, Tracerline) that was transported with the fuel and spray processes. The dye has a flashpoint of 131°C, which is above the calculated wall temperature. A 75 ppm concentration of dye was used in each fuel. Laboratory analysis by Coordinating Research Council member companies has shown that no appreciable measurable changes to the dyed fuel properties at a 75 ppm dye level could be measured using standard ASTM characterization techniques.

Specifically, EEE HFO437 Tier II certification fuel from Haltermann products with and without the 75 ppm dye was tested using: ASTM D6729 Detailed Hydrocarbon Analysis (DHA) by Gas Chromatography (GC), D5580 Aromatics in Gasoline by GC, D86 Distillation, D5191 Vapor Pressure of Gasoline by Mini at 100°F, D2699 Research Octane Number (RON) by Engine, D2700 Motor Octane Number (MON) by Engine, D240 Heat of Combustion by Bomb Calorimeter, D4052 Density by Digital Meter, D7191 Hydrogen by Proton NMR, D4629 Nitrogen by Oxidative Combustion with Chemiluminescence, and D5453 Sulfur by Oxidative Combustion with Ultraviolet Fluorescence (UVF). For the above noted tests, all results for fuels with and without dye were within the reproducibility of the test methods. All results were also within the repeatability of the test methods except for D240 Heat of Combustion and D4052 Density. Additionally, initial results of sump oil fuel dilution are in notional agreement with the FiL diagnostic results, with full physically measured oil sump fuel dilution results and analysis pending.

A schematic of the FiL instrument developed by Neupane et al. [39] is shown in Figure 1. It used a 532 nm continuous-wave laser (Lasever Inc. LSR532NL) as an excitation source, followed by a beam splitter that divides the laser into two beams. This feature enabled using two probes simultaneously as explained in the engine setup subsection. The probes consisted of 6-around-1 optical fiber assemblies; the center 1 fiber was used to guide the excitation laser light to the sample, and the 6 surrounding fibers collected and guided the fluorescence light to the spectrometers (Ocean Insight FLAME-T), which resolved the laser-induced fluorescence spectra.

The FiL instrument and calibration were previously demonstrated to be robust over a broad range of engine operating conditions and fuels [39]. Previous results showed that the 75 ppm dye level provided strong signal to noise and prevented signal saturation during low-speed preignition measurements [39, 42].

FIGURE 1 Schematic of FiL instrument setup showing 532 nm laser, dual 6-around-1 fiber-optic probes, and spectrometers.

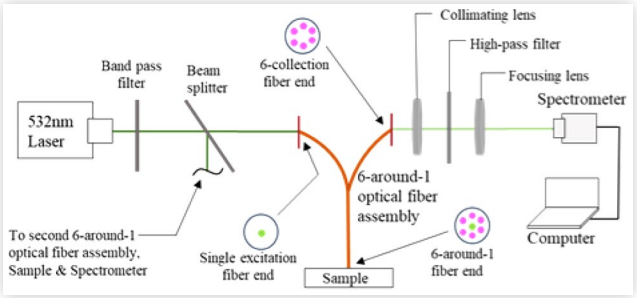

© UT-Battelle, LLC

Engine

A SCE derived from a production GM 2.0L ECOTEC LNF engine was used for the present work. The transformation from a production engine to an SCE was possible through deactivating three of the four cylinders (cylinders 1–3) of the engine. The geometry of the combustion chamber and camshaft profile for the fired cylinder remained stock. The production side–mounted direct injector was operated at 100 bar of fuel pressure constantly during the experiments. The engine specifications are presented in Table 1.

Figure 2 shows the layout of the engine setup, highlighting the dry sump oiling system used. The engine is attached to an alternating current dynamometer of 60 hp power capability, which can both motor and absorb engine power to maintain speed at the desired steady-state operating conditions. To mitigate the pulses typical of SCEs, the stock flywheel was replaced with an oversized flywheel (12 in. diameter, 3 in. thick) made of solid steel.

A mass flow controller (ALICAT 2000 SLPM) was used to supply air from an external air compressor to the engine. The air was conditioned with humidity below 5% using an air dryer, and the air temperature was fixed at 35°C using a heater. The air dryer, heater, and air mass flow controller were placed upstream of a surge tank located prior to the intake plenum. Exhaust backpressure was controlled by a backpressure valve

TABLE 1 Engine characteristics

Bore (mm)	86
Stroke (mm)	86
Connecting rod (mm)	145
Compression ratio	9.2:1
Number of valves	4
Displaced volume (L)	0.495
Exhaust valve lift (mm)	10.3
Exhaust valve duration at 1.27mm lift (°CA)	188
Inlet valve lift (mm)	10.3
Intake valve duration at 1.27mm lift (°CA)	200
Direct injector	Side-mounted
Rail pressure (bar)	100

© UT-Battelle, LLC

FIGURE 2 Schematic of engine dry sump oil system with FiL measurement points highlighted.

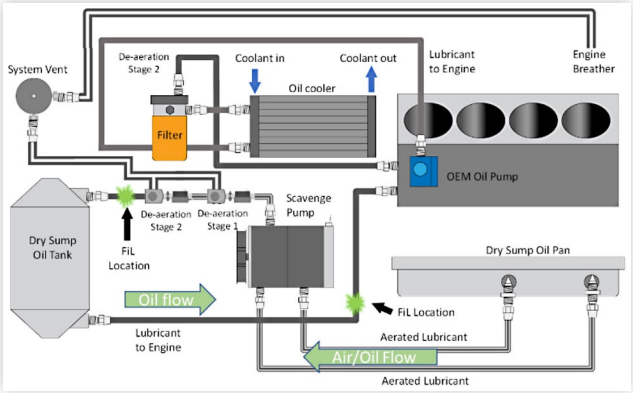

© UT-Battelle, LLC

(Flowserve Series 75) installed downstream of the exhaust surge tank and maintained a constant positive ΔP of 15 kPa between the intake and exhaust plenums (intake higher than exhaust). Controlling ΔP enabled the system to replicate real turbocharging conditions as the combined turbocharger efficiency remained at approximately 35% for all experiments [43].

Air-to-fuel ratio was monitored using a pressure-compensated Lambda sensor (ECM EGR 5220) installed in the laboratory-specific exhaust manifold. The air—to—fuel ratio was also calculated simultaneously using the commanded air mass flow, a Coriolis-based fuel flow meter (Micro Motion ELITE CMF010P), and emissions bench measurements to account for carbon and oxygen content of the exhaust flow.

Fuel supply was provided using two different systems. A low-pressure lift pump system was used to supply the production high-pressure direct injection fuel pump. The lift pump fuel system consisted of a fuel pump (Mallory Series 140) to extract fuel from a 55 gal. drum and feed a high-flow fuel pump (Aeromotive 11124) coupled to a pressure fuel regulator (Aeromotive 13128) rated at 3 bar. Unused fuel was recirculated from the fuel pressure regulator through a heat exchanger back to the lift pump maintaining the fuel temperature at a target temperature of less than 35°C. An external coolant pump, which was coupled to a tightly controlled heat exchanger, was used to control engine coolant and oil temperatures at a constant level.

The engine lubrication system was extensively modified in this work to enhance the sensitivity of oil dilution measurements. The production engine oil pump was maintained, but the engine was retrofitted with a dry sump oiling system and external oil sump. This increased the dry sump-out FiL sensitivity because the measurement is made from the scrape down oil sample before dilution with the bulk sump oil, as shown in Figure 2. A second FiL measurement point was added to simultaneously monitor oil flow coming to and from the engine, as shown in Figure 2. The stock oil cooler was replaced by an external oil cooler with higher capacity coupled to the coolant system to condition the oil temperature, maintaining a constant 90°C. A two-stage dry sump scavenge system was used to evacuate the crankcase. On the way to the external 3 gal. bulk-oil reservoir, a two-stage deaeration process was used by installing two centrifuge (Spintric III) devices in series. Deaeration of the oil flow is critical for the FiL instrument since excess air in the oil flow affects the signal. Therefore, the dry-sump-out FiL (oil flow from the engine) probe was installed after the second deaeration stage and before the bulk-oil reservoir; a second engine-supply FiL probe (oil flow to the engine) was positioned between the reservoir and the OEM oil pump.

Engine control and data acquisition was conducted by a National Instruments Combustion Analysis Toolkit (DCAT) tool. In-cylinder pressure was measured by a Kistler pressure transducer (6054BRU59), and engine speed was acquired by an AVL encoder (365C01) with a crank resolution of 0.2°CA.

Fuels

Four fuels (Fuel 1, 2, 3, 4) were used in this study, and their properties are listed in Table 2, where all fuels were tested without fuel additives. All fuels are based on either the neat form of or a splash blend of tetralin and/or ethanol into a 96 RON Tier II E0 fuel (fuel 1). All fuels were procured from Gage Products where the splash blends are 5% by vol. tetralin (Fuel 2), 25% by vol. ethanol (Fuel 3), or 25% by vol. ethanol plus 5% by vol. tetralin (Fuel 4).

Lubricant

The experimental campaign used an API and OEM approved 5W-30 oil widely used in the North American market. Two batches of lubricant were prepared for the experimental campaign with pertinent measured properties in Table 3. To ensure the FiL signal quality throughout the experiments, the oil and filters were changed for every set of segments performed. This procedure mitigated lubricant carry-over effects by using fresh lubricant for every case run.

Combustion Analysis

Combustion analysis was carried out using a MATLAB routine made in-house. It is based on in-cylinder pressure and applies a zero-phase filtering and a cycle-specific crank-position phasing correction prior to analysis. The stock cam profile is used to resolve the trapped residuals on a cycle-to-cycle basis following the approach proposed by Cavina et al. [44]. Although this approach allows exhaust gas recirculation effects to be quantified, this was not considered in this study. In-cylinder losses were calculated by using two models. Thermal losses were accounted following the approach proposed by Woschni et al. [45], and the losses due to crevices volume were accounted by using the approach proposed by Gatowski et al. [46]. These subroutines were applied in series to resolve the heat release rate.

Top dead center (TDC) was determined based on the shape of the heat release rate when motoring the engine and was estimated using the approach proposed by Tunestål et al. [47]; the analysis uses heat-loss power through the cylinder liner walls, which is assumed to be constant during motoring in the vicinities of TDC. This TDC analysis was consistent with separate TDC measurements using a magnetic proximity probe (AVL OT-SENSOR 428).

SPI Characterization

The combustion analysis routine was updated with a dedicated subroutine for identifying SPI events and resolving all metrics and statistics required to study them. Potential SPI cycles were identified using the approach described by Mansfield et al. [48]. The present approach identified SPI cycles that exhibited statistically significant early combustion as defined by the 2 percent mass fraction burned crank angle (CA02). Although SPI can occur with both large peak pressure and early combustion, this study employed only early CA02 as the definition of SPI. The rationale for only CA02 based analysis was founded in that peak pressure based and the conflation of peak pressure and early CA02 based SPI identification routines were also employed in the analysis, but the findings of these metrics in this study (i.e., this engine, operating conditions, and fuels used) were found to be practically identical, thus for simplicity only CA02 data will be presented herein.

TABLE 2 Fuel properties

	Fuel 1	Fuel 2	Fuel 3	Fuel 4
MON (ASTM D2700)	89.2	88.3	91.2	90.9
RON (ASTM D2699)	98.1	98.1	104.5	103.9
Anti-Knock Index [(R+M)/2] (ASTM D4814)	93.6	93.2	97.9	97.2
IBP (°F) (ASTM D86)	87.3	88.2	92.0	95.2
T5 (°F) (ASTM D86)	113.8	112.8	118.9	118.1
T10 (°F) (ASTM D86)	130.2	131.9	130.0	132.8
T20 (°F) (ASTM D86)	152.0	155.4	142.9	146.5
T30 (°F) (ASTM D86)	177.2	182.5	153.8	156.9
T40 (°F) (ASTM D86)	204.6	209.8	161.1	163.2
T50 (°F) (ASTM D86)	221.6	225.9	165.0	166.0
T60 (°F) (ASTM D86)	230.1	236.5	167.3	168.2
T70 (°F) (ASTM D86)	239.8	250.5	184.1	213.8
T80 (°F) (ASTM D86)	260.0	282.5	245.1	262.6
T90 (°F) (ASTM D86)	316.3	343.9	297.3	339.5
T95 (°F) (ASTM D86)	338.6	368.5	331.4	368.2
FBP (°F) (ASTM D86)	364.5	388.3	369.3	394.0
Residual (vol %) (ASTM D86)	0.9	1.1	0.8	0.8
Drivability Index (°F)	1187	1224	985	-
Time, Initial Boiling Point (sec.) (ASTM D86)	422	429	443	423
Time, Initial Boiling Point to 5% (sec.) (ASTM D86)	92	90	94	93
Time FH to Final Boiling Point (sec.) (ASTM D86)	181	132	180	213
Free/visible water (-) (ASTM D86)	Absent	Absent	Absent	Absent
Total Vapor Pressure (PTOT) (PSI) (ASTM D5191)	9.72	9.88	10.42	9.93
Vapor Pressure, EPA (psi) (ASTM D5191)	8.98	9.09	9.55	9.07
Vapor Pressure, ASTM (psi) (ASTM D5191)	8.74	8.87	9.38	9.02
Dry Vapor Pressure Equivalent at 100°F (psi) (ASTM D5191)	8.92	9.10	9.62	9.05
C2 (vol %) (ASTM D6730M)	0.000	0.000	22.560	23.489
C3 (vol %) (ASTM D6730M)	0.000	0.000	0.003	0.000
C4 (vol %) (ASTM D6730M)	2.791	3.104	1.894	1.900
C5 (vol %) (ASTM D6730M)	24.461	23.177	18.699	19.154
C6 (vol %) (ASTM D6730M)	2.818	2.654	3.145	2.258
C7 (vol %) (ASTM D6730M)	21.599	20.386	16.881	14.843
C8 (vol %) (ASTM D6730M)	29.771	28.023	21.870	20.222
C9 (vol %) (ASTM D6730M)	12.406	11.678	9.588	8.471
C10 (vol %) (ASTM D6730M)	3.771	6.752	2.991	7.971
C11 (vol %) (ASTM D6730M)	1.583	1.530	1.219	0.891
C12 (vol %) (ASTM D6730M)	0.208	0.202	0.090	0.097
C13 (vol %) (ASTM D6730M)	0.001	0.000	0.000	0.004
Carbon Sum (vol %) (ASTM D6730M)	99.408	97.506	98.941	99.298
PMI (-)	1.389	1.297	1.032	1.882
Carbon (wt %) (ASTM D5291)	86.51	86.7	77.43	77.62
Hydrogen (wt %) (ASTM D5291)	13.49	13.3	13.32	13.31
Oxygen (wt %) (ASTM D5622)	<0.1	<0.1	9.25	9.07
Net heating value (MJ/kg) (ASTM D240)	43.29	43.37	39.03	38.1
Ethanol (vol %) (ASTM D4815)	—	—	23.816	25.64
Other oxygenates (vol %) (ASTM D4815)	—	—	0.023	0.00
Total oxygenates (vol %) (ASTM D4815)	—	—	23.838	25.64
Density (g/ml @15.56°C) (ASTM D4052)	0.7447	0.7559	0.7557	0.7665
Specific gravity (@15.56°C) (ASTM D4052)	0.7458	0.7570	0.7571	0.7648

TABLE 3 lubricant properties

	Batch 1	Batch 2
Kinematic Viscosity at 100°C (cSt)	10.49	10.49
Kinematic Viscosity at 40°C (cSt)	61.87	-
High temperature High Shear at 150°C (cP)	-	3.17
Cold Cranking Viscosity at -30°C (cP)	-	6059
Ca (ppm)	1170	1170
Mg (ppm)	821	821
P (ppm)	751	751
S (ppm)	2471	2471
Zn (ppm)	872	872

In the analysis, data was checked for skewness and kurtosis and found that for all data sets presented herein normality of the data distribution was valid. The threshold for statistical significance was defined as four standard deviations from the mean in the CA02, which was established though normality verification of the data, and outlier thresholding. For this data set, four standard deviations were determined to be a robust threshold for outlier identification (i.e., CA02 SPI identification).

Cycles with CA02 occurring earlier than four standard deviations from the mean were identified as SPI cycles. Once identified, the SPI cycles were binned, and the associated mean values of the non-SPI cycles were calculated (i.e., mean and standard deviation values do not contain cycles with identified SPI events). Thus, this approach effectively identified the SPI events that can cause catastrophic failure to the engine, including knock and super knock events that occur during SPI events. The total number of SPI events also included those occurring in a cluster, defined as SPI events separated by no more than 10 cycles.

Operating Conditions

The SPI experiments were run following the scheme shown in Figure 3, where 10 square-waved segments were run in automated operation. Each segment consisted of 5 min at low-load (5 bar $IMEP_g$) operation followed by 25 min. at high-load operation (the ~18.5 or ~20 bar $IMEP_g$ for the 185 or 200 kPa intake pressures, respectively). During high-load operation, the first 5,000 cycles were discarded because of the transient behavior, and the subsequent 20,000 cycles were used for analysis. The resulting data set used in the analysis was 10 segments of 20,000 cycles per segment. However, the reported data herein discarded the first segment of the 10-segment set to prevent contamination/carry over effects from previous runs. Thus, all data presented herein is from segments 2-10, corresponding to 180,000 recorded cycles. Recording such a high number of cycles ensured sufficient data for accurate statistical analysis.

SPI operating conditions are inherently associated with heavily boosted and often low-speed conditions. The present experimental campaign was performed at 2,000 rpm. The 32 "X" cells in Table 3 highlight the operating conditions and fuels investigated in the study. Two absolute intake pressure values (185 and 200 kPa) were investigated; the ΔP was held constant with the intake 15 kPa higher than the exhaust. The

FIGURE 3 Set of segments conducted under automated operation at SPI-prone conditions.

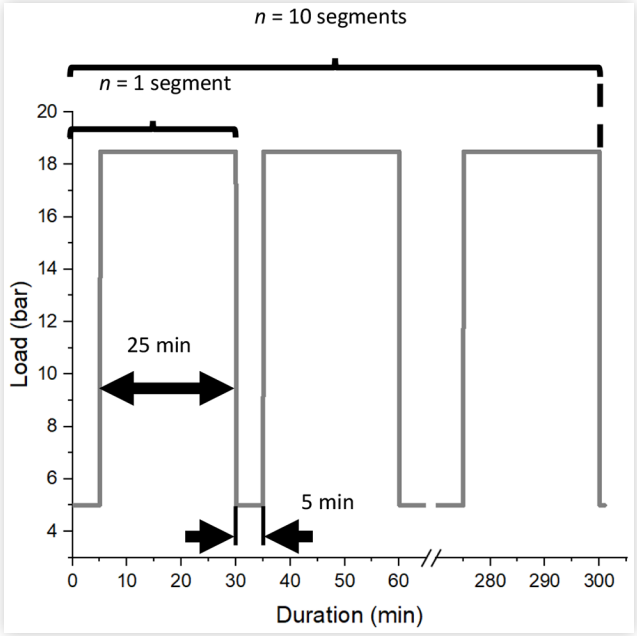

corresponding engine load achieved for the 185 and 200 kPa intake pressures was ~18.5 and ~20 bar $IMEP_g$, respectively. Two SOI timings and coolant temperatures were used in this study as described in Table 3; 310°CA and 220°CA $bTDC_f$, and 90°C and 70°C. For all conditions in Table 4, the CA50 timing was held constant at 33°CA after TDC by means of spark advance adjustments. Note that the SOI timings are nominal as the study physically retained the centroid of the injection command identical for all fuels; however, this modification has a minor effect as the differences in injection timings were within only a few crank angles of each other (i.e., 2-to-3°CA start of injection differences between the fuels).

Baseline Condition

A baseline condition was operated after four consecutive experiments. The baseline condition and associated results are described in detail in Appendix A.

TABLE 4 All operating conditions and fuels used

		70°C coolant		90°C coolant	
Fuel	Timing (°CA)	Intake pressure		Intake pressure	
		185 kPa	200 kPa	185 kPa	200 kPa
Fuel 1	310°CA SOI	X	X	X	X
	220°CA SOI	X	X	X	X
Fuel 2	310°CA SOI	X	X	X	X
	220°CA SOI	X	X	X	X
Fuel 3	310°CA SOI	X	X	X	X
	220°CA SOI	X	X	X	X
Fuel 4	310°CA SOI	X	X	X	X
	220°CA SOI	X	X	X	X

Results

The data presented herein are the SPI events identified by CA02 of a cycle being 4 standard deviations earlier than the mean. Although recorded and analyzed, the data from segment 1 was omitted in the analysis to reduce associated errors that could occur from carry-over based biasing effects occurring during previous tests with different fuels and/or operating conditions. The corresponding 180,000 cycle data sets (segments 2-10 of 20,000 cycle each) were analyzed as a single data set (i.e., all 9 segments analyzed as a single grouping/run). The results are divided into four subsections, which outline the fundamental processes and findings of SPI dependencies and fundamentals on fuel–wall interaction and associated FiL measurements.

Overall FiL and SPI Trends

Results of the total SPI events for each fuel and operating condition as a function of measured FiL rate are shown in Figure 4; in addition to presenting the combined results, the 310°CA SOI and 220°CA SOI results are separated in the stack plot. Evidently, the 310°CA SOI results show the overall lowest SPI activity, with all but one condition displaying fewer than 10 total SPI events over the 10-segment test duration (200,000 cycles total, with only segments 2-10, 180,000 cycles, used in the present analysis), with no observable structure in SPI event count as a function of measured FiL rate. Conversely, the 220°CA SOI data show increased SPI counts and a triangular envelope structure of SPI event counts nominally inversely proportional to FiL rate—a non-intuitive finding. Moreover, the 220°CA SOI data show an increased FiL rate magnitude, ~1.5× that of the 310°CA SOI results, confirming that when the injection timing is delayed, more fuel–wall impingement occurs.

The combined results of each SOI condition are shown in the bottom plot in Figure 4, where the inverse dependency on SPI as a function of FiL and higher FiL rates of the 220°CA SOI condition are superimposed on the reduced SPI event count and reduced FiL rate 310°CA SOI data. The findings of inversely proportional SPI rate as a function of FiL rate in Figure 4 present a paradox of a generally accepted hypothesis on the mechanisms of SPI, where increased fuel–wall wetting is thought to be responsible for increased SPI rates. Clearly, simply measuring FiL alone without any analysis is insufficient if not inverse to the hypothesized fundamental dependencies of SPI propensity. To determine the source of the opposite trend observed in this study, further analysis was performed and presented in the subsequent sub-sections.

FIGURE 4 Unique SPI event count as a function of FiL rates for 310°CA SOI timing (top), 220°CA SOI timing (middle), and both SOI timings combined (bottom).

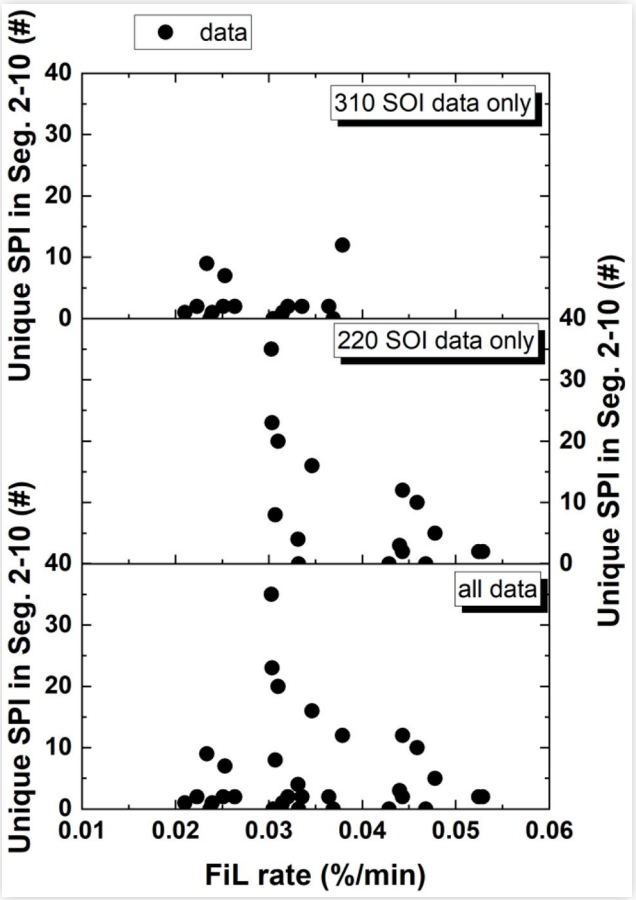

Fueling Rate Effects on FiL, Carbon Balance, and SPI

The SPI results for the various operating conditions and fuels were sorted by coolant/oil temperature and SOI and are presented in Figure 5, which also partitions the data by fuel type using different marker colors. When partitioned as shown in Figure 5, the data trends start to become more obvious. Specifically, for each SOI/temperature combination, the SPI events for the fuels with 25% ethanol (E25, E25/T5) occur at a ~40% greater FiL rate than the E0 fuels (base and T5). Thus, the SPI events for fuels with 25% ethanol occurred at a ~40% greater FiL rate, indicating that they occurred under conditions with substantially higher fuel–wall interaction compared with the E0 fuels.

In Figure 6, the fueling and FiL rates of the data in each quadrant of Figure 5 were independently normalized by dividing each fuel at each SOI/coolant temperature condition (i.e, each quadrant in Figure 5) by the conditions respective minimum fueling rate. Then the normalized data was zero offset shifted by subtracting the respective minimum value for each quadrant from each fuel. Likewise, the FiL rate was normalized in a similar manner. Processing the data in this approach generates the relative increase in FiL and fueling rate independently for each SOI/temperature condition, enabling direct comparison.

Although Figure 6 shows that the E25 fuels require a ~13% increase in fueling duration compared with the E0 fuels at their respective boost levels (note two boost levels plotted in each quadrant), the corresponding normalized FiL rates of the E25 fuels far exceed a 13% increase. Thus, Figure 6 highlights that fuel–wall impingement rates with the E25 fuels are

FIGURE 5 Unique SPI event count as a function of FiL rate for 310°CA SOI timing (top row), 220°CA SOI timing (bottom row), 90°C coolant temperature (left column), and 70°C coolant temperature (right column). Data markers are color-coded by fuel; boost levels are not delineated. Note Fuel 1 and 2 are E0 fuels, and Fuel 3 and 4 are E25 fuels.

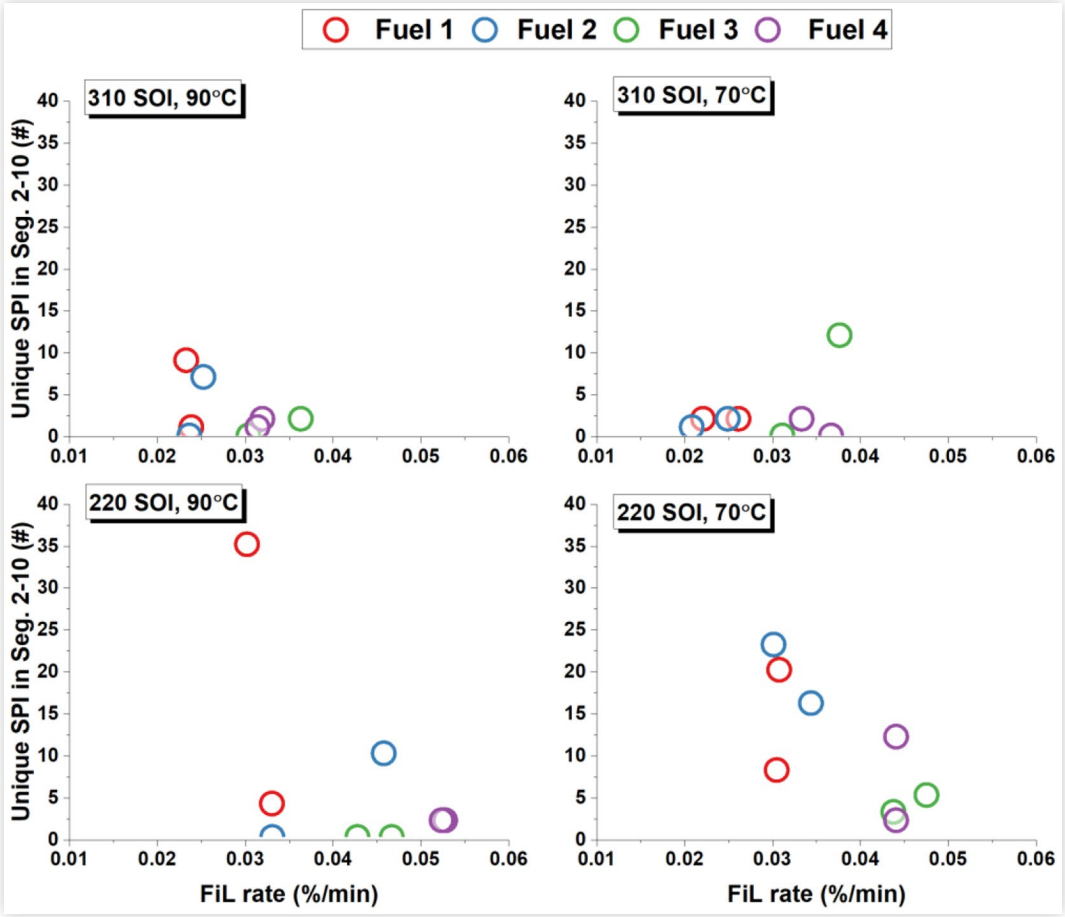

far beyond those that can be attributed to energy density variation alone.

The results in Figure 6 show that at each SOI/temperature condition where SPI occurs, the minimum fueling rate and FiL are coincident, meaning that they are also codependent (i.e., minimum fueling corresponds to minimum FiL). Moreover, the results of Figure 6 also show that the relative increase of FiL rate for the E25 and E25/T5 fuels is approximately 2 to 3 times higher than the relative increase in fueling rate increase required for these fuels. Thus, Figure 6 highlights that additional variables/factors affect the increased FiL rate with the E25 fuels beyond the heating value–based differences alone.

The SPI propensity as a function of excess fueling required was also examined. No correlation between the fueling rate increase and SPI rate was observed, indicating that a carbon balance on the engine alone was not sufficient to indicate SPI propensity in this study.

Figure 6 clearly shows that with fuels 3 and 4 (E25-fuels), FiL rates increase more than would be predicted by the difference in heating value of E25 alone. However, the figure does not clarify whether the disproportionally high increase in FiL rates with fuels 3 and 4 are simply fuel impingement or fuel retention. In other words, the question remains, does increased FiL rate correspond to increased fueling rates because of "lost fuel" to the crankcase, and if so, why is the SPI trend in Figure 5 so much lower for fuels 3 and 4?

To answer these questions, the FiL and SPI results were plotted against excess fueling rate required to achieve Lambda = 1 exhaust stoichiometry. Excess fueling rate is defined in Eq. 1, where AFR_{stoic} is the stoichiometric air fuel ratio of the fuel as determined by the measured fuel carbon, hydrogen, and oxygen weight percentages, $\lambda_{exhaust}$ is the measured exhaust lambda (i.e., 1 for all tests herein), and AFR_{mass} is the measured air fuel ratio defined by the measured mass of air and fuel delivered to the engine.

$$Excess\ Fueling\ Rate = \lambda_{exhaust} - \frac{AFR_{mass}}{AFR_{stoic}} \quad (1)$$

Figure 7 and Figure 8 show the FiL rate and SPI results, respectively. These results reinforce the findings of Figure 6, in that excess fueling rates to maintain Lambda = 1 exhaust is not correlated well with FiL rates. Therefore, the carbon balance of the engine alone is insufficient to describe physical fuel–wall impingement propensity and associated fuel/oil dilution effects.

Moreover, Figure 8 reinforces that because there is no observed dependency of SPI propensity on excess fueling

FIGURE 6 Normalized FiL rate increase as a function of normalized fueling rate for 310°CA SOI timing (top row), 220°CA SOI timing (bottom row), 90°C coolant temperature (left column), and 70°C coolant temperature (right column). Data markers are color-coded by fuel; boost levels are not delinated. Note Fuels 1 and 2 are E0 fuels, and Fuels 3 and 4 are E25 fuels.

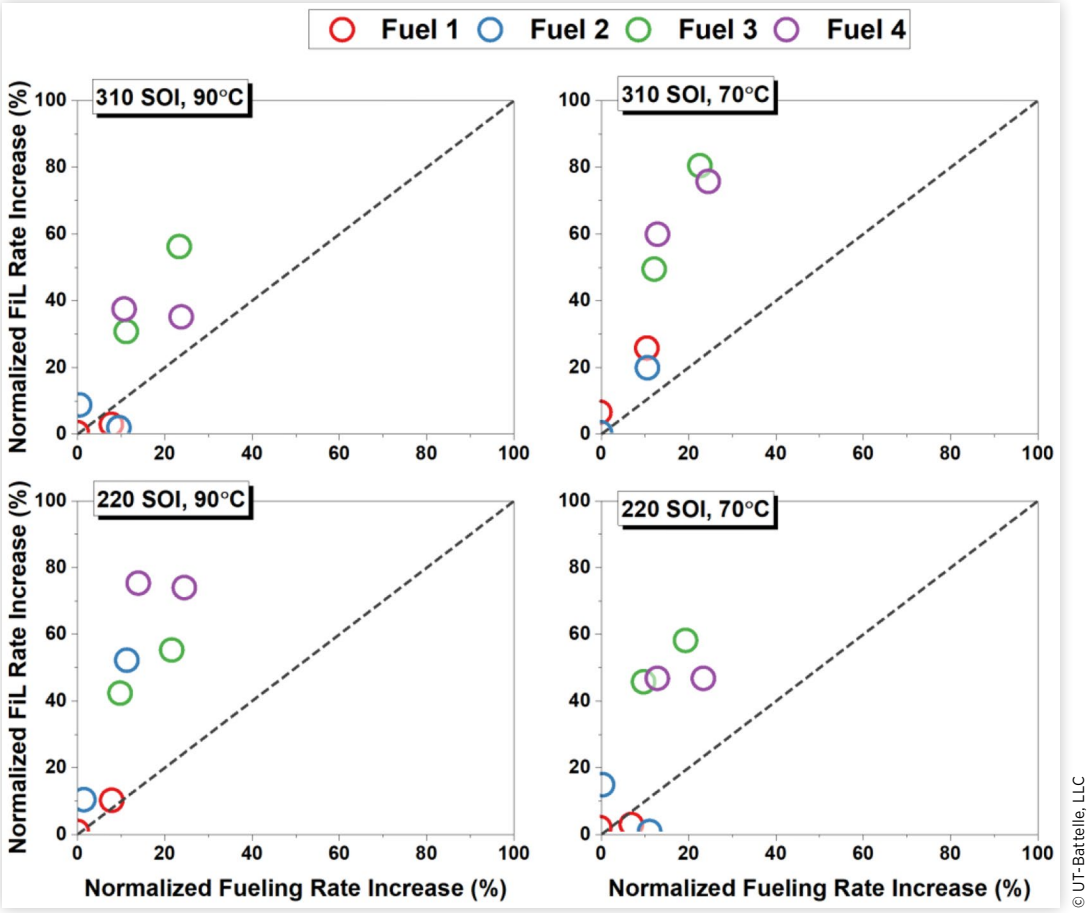

required, the engine carbon balance alone is insufficient to fully represent the physical processes generating TRZ ignition sources of SPI. Regardless of this shortfall, fuel-specific trends and observations can be gleaned from Figure 7 and Figure 8.

In Figure 7, fuels 3 and 4 (the E25 fuels) clearly exhibit increased FiL rates. This suggests, like the results of Figure 6, that increased FiL from the E25 fuels results from a physical difference in these fuels. Previous studies by Splitter et al. [37] have suggested that high-volatility fuels can exhibit spray collapse, especially at the 220°CA SOI condition. Moreover, Hwang et al. [49] has demonstrated that ethanol-containing fuels exhibit spray collapse processes, which can increase fuel–wall impingement. Based on these previous works and similar measurements, a fundamental driving force causing the greater E25 fuel FiL rates is likely the increased propensity for these fuels to have collapsing sprays, especially at the 220°CA SOI timing.

Additionally, Figure 7 demonstrates that the T5 fuels, regardless of ethanol content, exhibit the highest excess fueling rates required (i.e., the greatest carbon balance error to maintain Lambda = 1 exhaust, meaning the most retained/lost fuel in the engine). Thus, although Figure 7 does not directly show a relation between excess fueling and FiL rate, it does show that fuel physical properties are grouped in this study. Specifically, the T5 fuels require the most excess fueling, and the E25 fuels exhibit the highest wall wetting, but these factors are not directly dependent on each other.

If the highest FiL and largest excess fueling required were intrinsically linked to each other and SPI, then the E25/T5 fuel at 70°C coolant and 220°CA SOI would exhibit the highest SPI propensity, which is inverse of the SPI count in Figure 5, where the E25/T5 fuel is the second lowest at this condition (E25 is the lowest). Therefore, there is likely a fuel-specific effect, which appears to not be fully captured from excess fueling rates and FiL alone.

Likewise, Figure 8 shows no direct dependency on SPI propensity as a function of excess fueling rate required for Lambda = 1 exhaust. Therefore, combining this knowledge with the FiL trends in Figure 5 and previous figures, this study found no direct links in readily measured factors that directly correlated SPI with carbon balance or fuel–wall wetting. There was an observable trend in FiL being dependent on volatile fuel species (E25), and there was a trend in higher–boiling point fuel species (T5) exhibiting increased carbon balance errors (higher fueling rates needed for Lambda = 1 exhaust), suggesting higher retention rates in the engine for those fuels. Specifically, SPI was not observed to be uniquely correlated with either of these factors.

FIGURE 7 Excess fuel required for Lambda = 1 exhaust (i.e., carbon balance) as a function of FiL rate for 310°CA SOI timing (top row), 220°CA SOI timing (bottom row), 90°C coolant temperature (left column), and 70°C coolant temperature (right column). Data markers are color-coded by fuel; boost levels are not delinated.

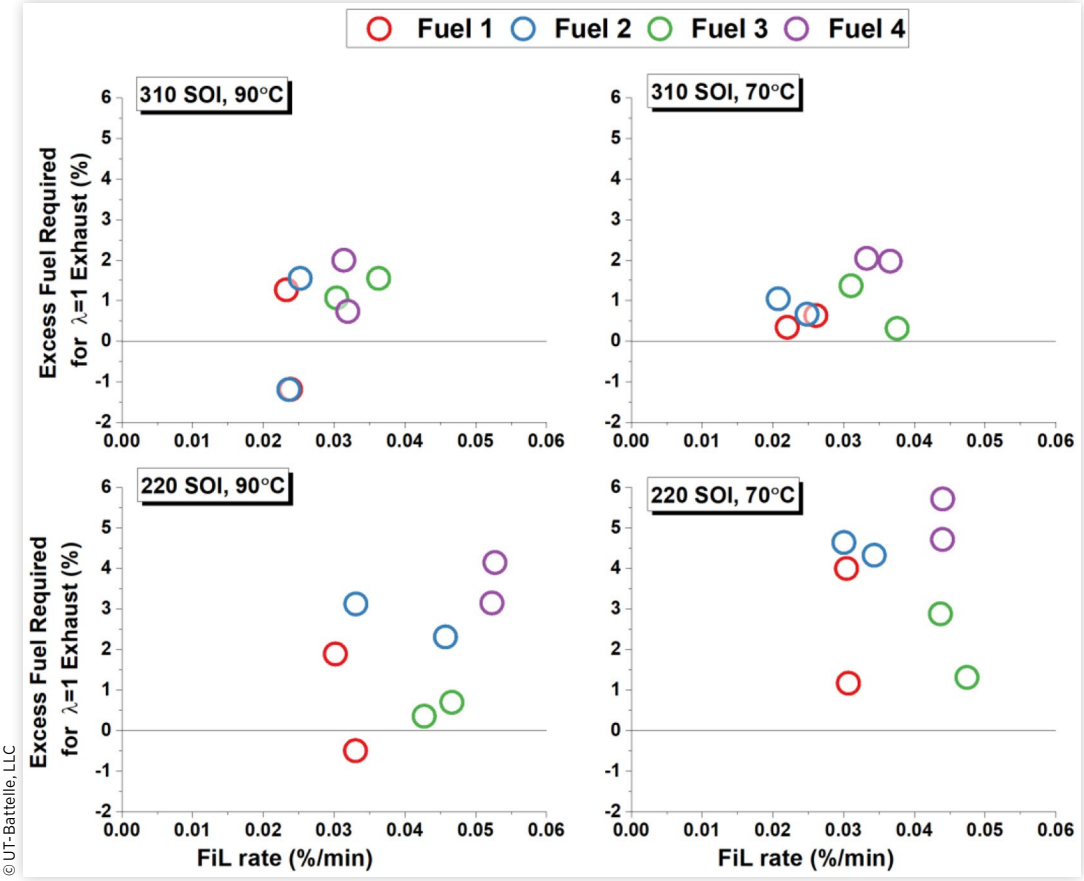

The fuel property specific effects shown in Figure 8 suggest that there are combined factors of increased fuel retention with fuels 2 and 4 (the T5 fuels), and increased FiL with fuels 3 and 4 (the E25 fuels). Previous studies by Meyer et al. [22] have suggested that SPI might be correlated to the portion of the fuel distillation above a certain temperature. In Meyer et al. [22], a linear temperature of 150°C was assumed; however, the present work uses lower assumed temperature based on findings for this engine presented in Mills et al. [50], which suggests closer to 100°C is more appropriate for the conditions presented herein.

Fuel Impingement and Post-Impingement Evaporation Theory and Quantification

From a first-principles conceptual approach, fuel that impinges on combustion chamber surfaces can only evaporate off those surfaces if the surface temperature is at or above the fuel's boiling point. For this evaporation to occur on a cycle-by-cycle basis, this assumption also requires that the boiling/evaporation process is rapid, on the order of crank angles, and the thermal capacity of the combustion chamber surface is much higher than that of the fuel. This concept is much easier to determine for single-component fuels because the distillation curve has a single temperature at which the fuels boil. For real multi-component fuels, this process requires an additional assumption that the fuel components with distillation temperatures above the combustion chamber surface temperature are unable to evaporate owing to insufficient temperature. A conceptual rendering of the impingement process is represented in Figure 9, where fuel–wall impingement is shown, as well as fuel mixing with lubricant films on the cylinder liner in the TRZ.

Although the schematic in Figure 9 depicts fuel impingement on both the cylinder liner and the piston, the FiL measurement requires physical migration of fuel from the combustion chamber to the engine oil sump, which must occur through the TRZ. Therefore, the FiL measurement captures the fuel that physically passed through the TRZ and did not evaporate. From the information in Figure 9 and the hypothesis that fuel components with boiling points greater than the wall temperature are thermodynamically prevented from evaporating, the FiL measurement is of fuel components that have boiling points higher than the wall temperature.

To determine the wall temperature for the present work, results of a complex conjugate heat transfer study on engine materials and surface temperatures by Mills et al. [50] were examined. The physical measurements used by Mills et al.

FIGURE 8 Unique SPI event count as a function of excess fuel required for Lambda = 1 exhaust (i.e., carbon balance) for 310°CA SOI timing (top row), 220°CA SOI timing (bottom row), 90°C coolant temperature (left column), and 70°C coolant temperature (right column). Data markers are color-coded by fuel; boost levels are not delinated.

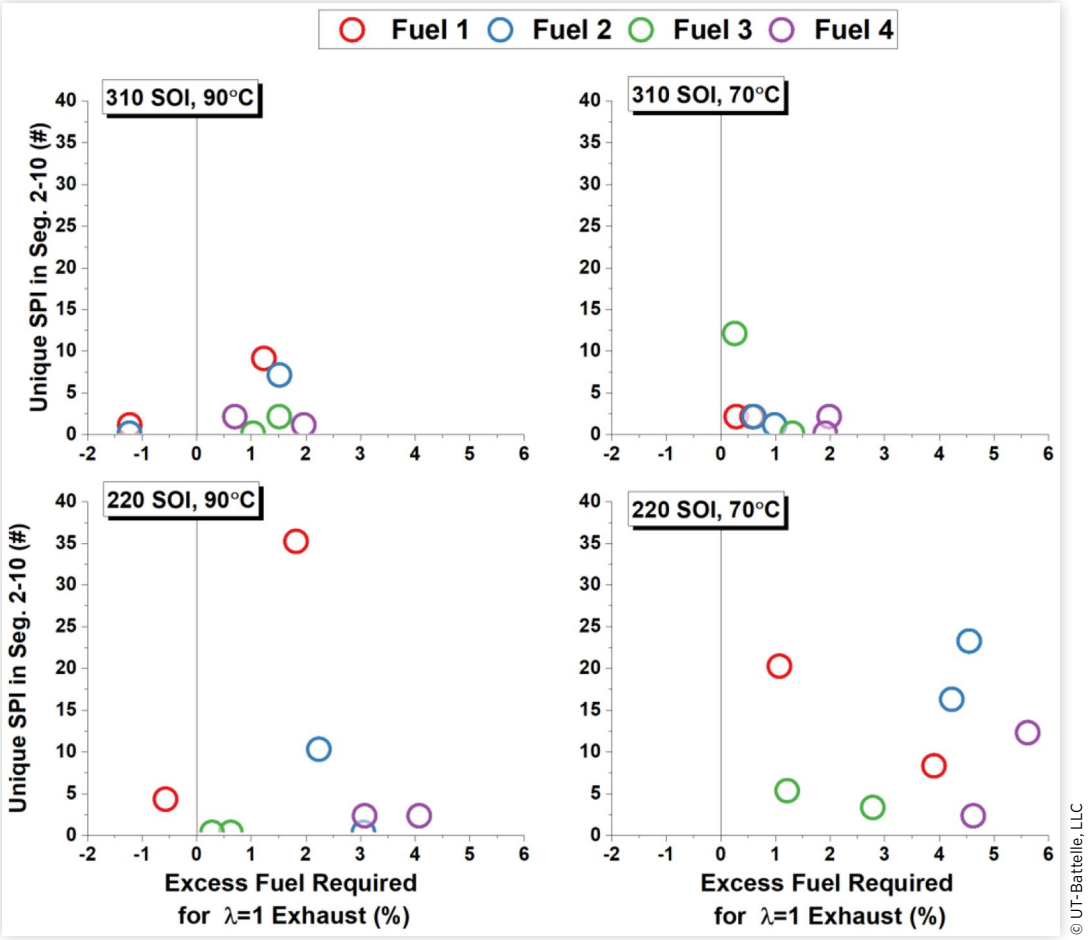

[50] for model calibration were from studies taken at the US Department of Energy's Oak Ridge National Laboratory using a physically identical experimental setup as used in the current work. In the findings by Mills et al., the cylinder liner temperature for 90°C coolant on the identical GM LNF engine at 2,000 rpm varied between 97°C and 107°C at 5 bar brake mean effective pressure operation, and between 97°C and 109°C for 15 bar BMEP operation, showing near zero linear temperature dependency on engine load. Based on these results, and that the present work is only above 15 bar BMEP operation, the wall temperature for all 90°C coolant condition experiments was assumed to be a constant 110°C. The wall temperature for the 70°C coolant condition experiments was assumed to be a constant 100°C. These threshold temperatures were selected based on the data from Mills et al. [50], from private communication with the authors, and from examining the best fit to the experimental data in this study.

Using these two assumed wall temperatures of 110°C for the coolant temperature of 90°C, and the assumed wall temperature of 100°C for the coolant temperature of 70°C, the fraction of fuel boiled at the wall temperature was calculated. Figure 10 shows the ASTM D86 boiling curves for each fuel and fit of each curve using a 5°C linear interpolation scheme. Evidently, Figure 10 shows no appreciable deviation between the fit and measured distillation curves for any fuel, especially in the 80°C and higher range of interest.

The corresponding unboiled fuel fraction for each fuel in Figure 10 using the 100°C and 110°C assumed wall temperature thresholds is presented in Table 5. From the results, ~50% of the E0 fuels and ~25% of the E25 fuels remained unboiled at the assumed wall temperature thresholds. Thus, ~50% and ~25% of the impinging E0 and E25 fuels, respectively, would remain as a liquid film on the cylinder walls and lead to corresponding fuel retention. Higher fuel fractions could be retained, and compositional species interactions could alter the fuel–wall boiloff behavior, but as an empirical bound, the results in Table 5 were assumed for this study.

Figure 11 shows the results of this analysis for the SPI events of all fuels and operating conditions. Linear fit trends between FiL and unboiled fuel percentage were observed across the space. Moreover, for a given SOI, the slopes of the linear fits at each temperature are similar, suggesting that the threshold assumptions of 100°C and 110°C at least provide some solution similarities. Additionally, independent of coolant temperature, the slope of the 220°CA SOI data is approximately 20%–25% steeper than the 310°CA SOI data, suggesting that for a given unboiled fuel percentage (i.e., fuel composition and coolant temperature), there is approximately

FIGURE 9 Conceptual rendering of fuel–wall impingement and retention process occurring at SPI-prone conditions.

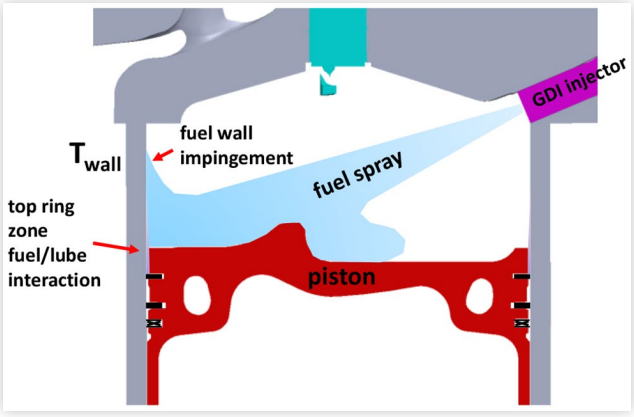

FIGURE 10 Measured ASTM D86 data (black lines) for each fuel plotted on inverse coordinates, with 5°C linear interpolation of each fuels data plotted as colored lines.

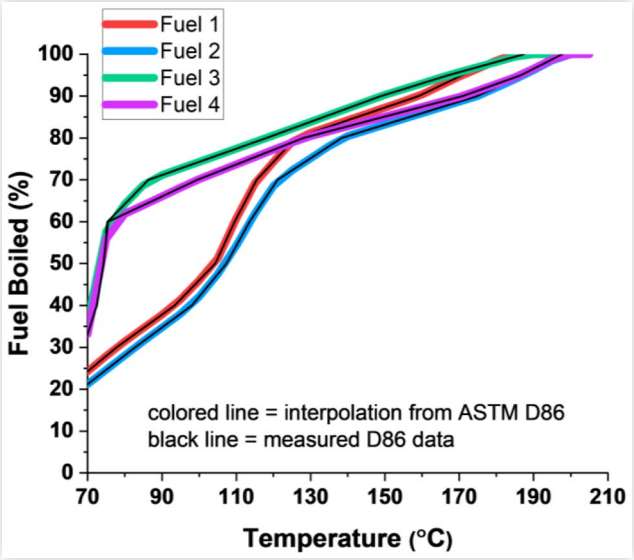

20%–25% more fuel impingement with the 220°CA SOI timing than with the 310°CA SOI timing.

Based on the strong linearity and trend-wise agreements in Figure 11, the FiL rate and unboiled fuel percentage were combined into a common term, *FIL**. The approach was performed for all SPI data and conditions independently using the unboiled fuel fractions (Table 5), with the respective measured FiL rate for each operating condition and fuel combination, as indicated in Eq. (2).

$$FiL^*_{fuel\,i} = FiL_{fuel\,i} * unboiled\ fuel\ fraction_{fuel\,i} \quad (2)$$

As defined in Eq. (2), *FIL** encompasses the effect of fuel impingement and the hypothesized fuel evaporation limit. Thus, *FIL** is a means to describe the fuel retained in the TRZ of the engine. As described previously, the flash point of the tracer dye is relatively high (131°C), meaning that it is highly improbable if not physically impossible for the dye to

TABLE 5 Unboiled fuel percentage calculated for each test fuel at each coolant temperature.

	70°C coolant (100°C wall temperature)	90°C coolant (110°C wall temperature)
Fuel 1	0.540	0.622
Fuel 2	0.579	0.653
Fuel 3	0.257	0.289
Fuel 4	0.298	0.336

evaporate off the engine cylinder liner. Therefore, the FiL instrument provides a sensitive measure of the fuel that physically impinged on the engine surface but does not account for the fuel fraction that boils off upon impingement. By multiplying the FiL rate by the fraction of fuel remaining in the liquid layer as in Eq. (2), *FiL** directly provides a metric of the fuel retained in the engine.

Figure 12 shows the SPI propensity as a function of *FiL**, which indicates a strong linear trend agreement for the fuel spray wall-targeting 220°CA SOI timings; greater *FiL** correlates with greater SPI. For the piston-targeted 310°CA SOI timings, nearly zero correlation is observed, as expected. Moreover, the slopes of the trend lines for the 220°CA SOI data are in agreement with the colder coolant temperatures enhancing fuel retention, as also indicated by the increased carbon balance errors in Figure 8.

Based on the intersection of the trend line results in Figure 12, the two coolant temperatures were combined, and the data were plotted as a function of FiL* for both SOI Figure 13. In examining the SOI trends and associated linear fit trend lines in Figure 13, the dependency of SPI events on *FIL** for this engine at these conditions with this operating test was ~0.01%/min (i.e., the intercept between 310°CA SOI and 220°CA SOI linear fit lines if the SOI results are superimposed on each other). Therefore, for SPI dependency on TRZ liquid to become active, a total fuel dilution of 0.25% in needed in each 25 min segment, or at least 2.5% fuel dilution in the TRZ over the entire 10 segment test (SPI for segments 2–10 plotted). Additionally, the 310°CA SOI timing results in Figure 13 highlight that the SPI noise floor of this engine is ~2.5 events for a 10 segment test, where deviations from that could be attributed to secondary effects such as filter smoke number, aerodynamic instability of deposits, or other non-FiL related phenomena.

Fuel Property Identifiers Influencing FiL*

The previous subsection highlighted that there is a strong agreement between *FiL** and SPI propensity, meaning that fuel impingement and retention is critical for SPI. The current work employed a nonconventional FiL diagnostic to obtain measurements of fuel–wall impingement. Although this is useful in a laboratory setting, it is not as readily deployable to a wider field of data or provide fuel property effect information a priori.

The concept of fuel distillation and retention on SPI was extended to examine if a fuel's PMI could be a surrogate to

FIGURE 11 FiL rate as a function of unboiled fuel percentage for 310°CA SOI timing (top row), 220°CA SOI timing (bottom row), 90°C coolant temperature (left column), and 70°C coolant temperature (right column). Data markers are color-coded by fuel; boost levels are not delinated.

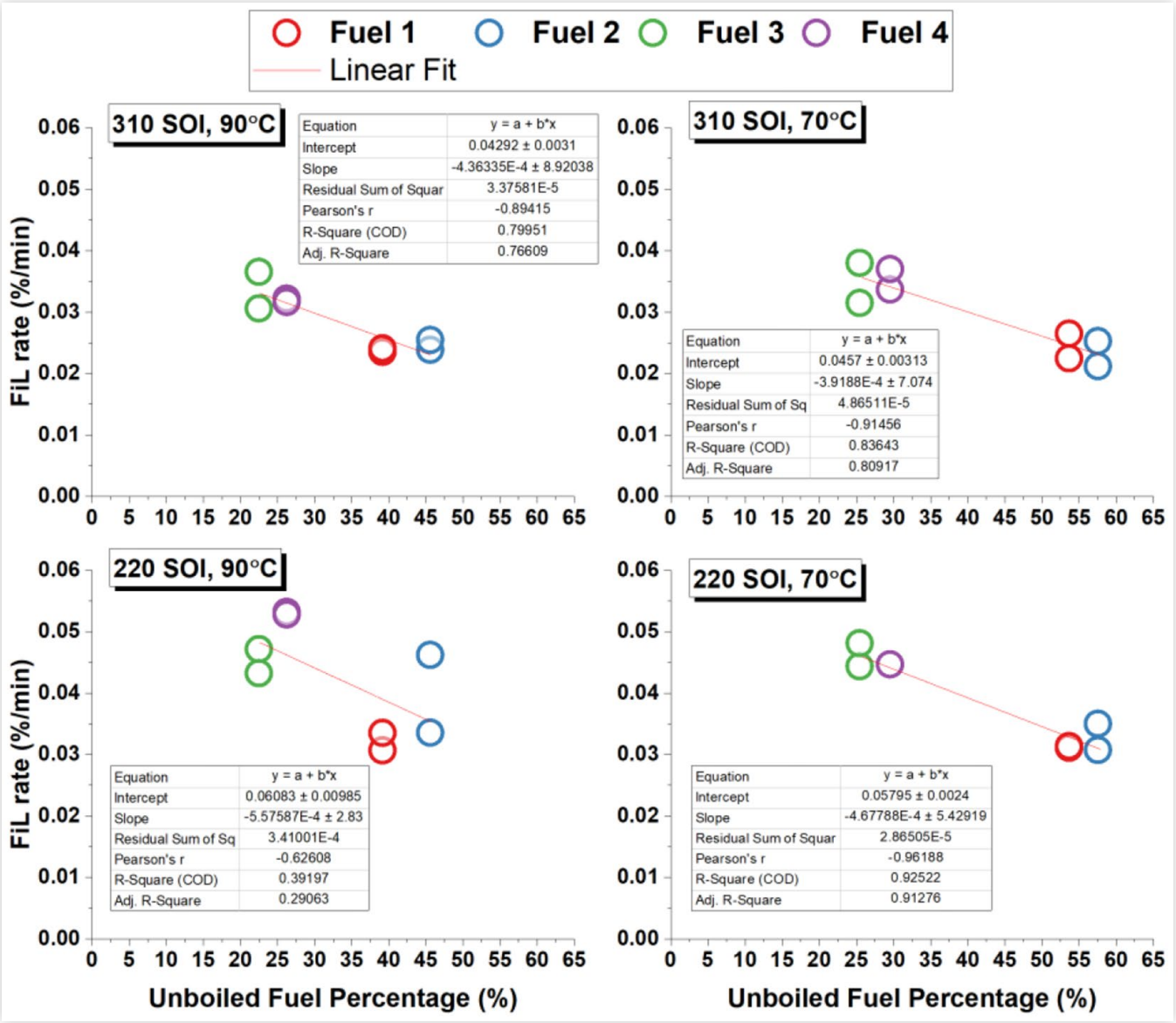

*FiL**. Figure 14 presents PMI on a detailed hydrocarbon analysis weight percentage basis relative to *FiL**. There was a fairly good agreement with the data, and a fairly linear trend was observed. However, diligent analysis shows that the E25/T5 and base fuels (purple and red markers, respectively) appear to be flipped in their relation to a linear trend. In other words, the base fuel has higher *FiL** and lower PMI than the E25/T5 fuel, which has a disproportionally higher PMI relative to *FiL**. Thus, although *FiL** and PMI appear to be related, the data are not directly comparable. Moreover, the PMI of the E25/T5 fuel is the second highest, but the SPI rates of that fuel are quite low. Thus, there are likely factors beyond PMI that affect SPI and *FiL**. Nevertheless, for this relatively small data sample, PMI generally indicates a proportional relation to *FiL** and thus SPI, but deviations do exist, especially with fuels exhibiting increased volatility below T50 and increased fuel retention above ~T70.

Summary/Conclusions

This work investigated fuel–wall interaction and its effect on SPI propensity. The hypothesis that changes in fuel properties impact fuel spray plume and fuel penetration length will result in fuel wall impingement. Using a laser induced florescence-based FiL diagnostic in the engine lubricant system and a dry sump oiling system, the fuel–wall interaction was measured during an SPI test protocol. Experiments with four fuels, each at two coolant temperature levels, two boost levels, and two

FIGURE 12 Unique SPI event count as a function of *FiL** for 310°CA SOI timing (top row), 220°CA SOI timing (bottom row), 90°C coolant temperature (left column), and 70°C coolant temperature (right column). Data markers are color-coded by fuel; boost levels are not delinated.

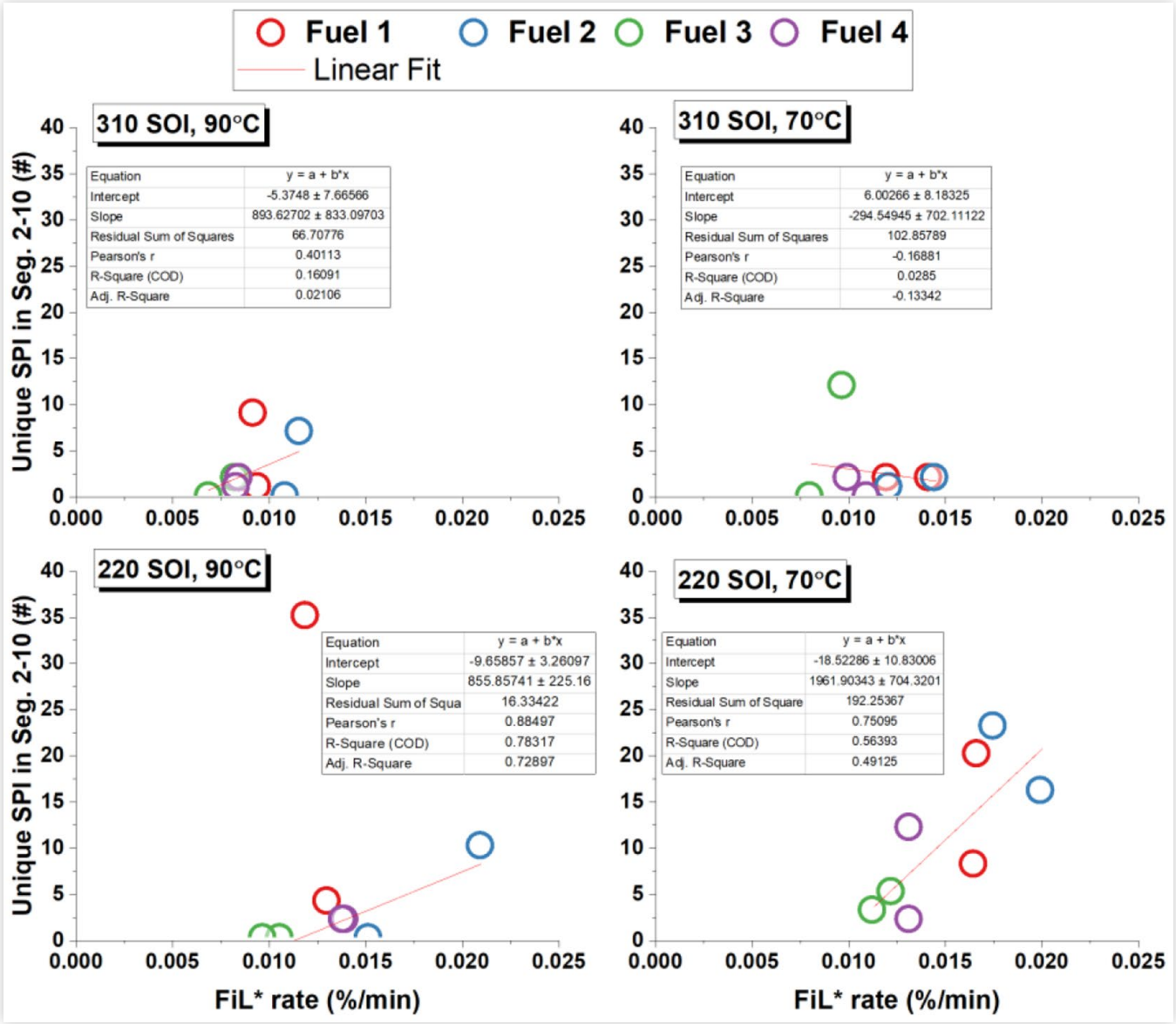

SOI timings, were examined. The results of SPI rate, fuel in oil, carbon balance, fueling rates, and fuel boiling properties were analyzed for dependencies. The major findings of the study are as follows:

- Laser induced florescence measurements of Fuel in Lube (FiL) rates as measured were inversely proportional to SPI activity. Physical effects of spray collapse and fuel volatility were attributed to increased fuel–wall impingement but increased evaporation of impinged high-volatility fuels.
- Carbon balance of the engine was not directly correlated with SPI, but T5 fuels increased the carbon balance error, suggesting that these fuels were more prone to reduced mixing and or post-impingement evaporation when impinged on engine surfaces.
- Using assumed cylinder liner temperature thresholds of 100°C and 110°C for the 70°C and 90°C coolant temperature conditions, respectively, a theoretical fuel retention fraction (i.e., unboiled fuel fraction) of impinged fuel was calculated based on ASTM D86 measurements of fuel distillation curves. The FiL rate of the engine was very linearly correlated with the unboiled fuel fraction.
- FiL measurements were modified to account for fuel retention by combining the measured FiL with the measured fuel distillation at the calculated cylinder liner temperature. The approach established the term *FiL**, which was calculated as a representative metric corresponding to suspected unboiled fuel on the linear that was retained in the top ring zone (TRZ). It accounts for both fuel–wall impingement and fuel fraction that

FIGURE 13 Unique SPI event count as a function of *FiL** for 310°CA SOI timing (top) and 220°CA SOI timing (bottom). Data markers are color-coded by fuel; boost levels are not delinated.

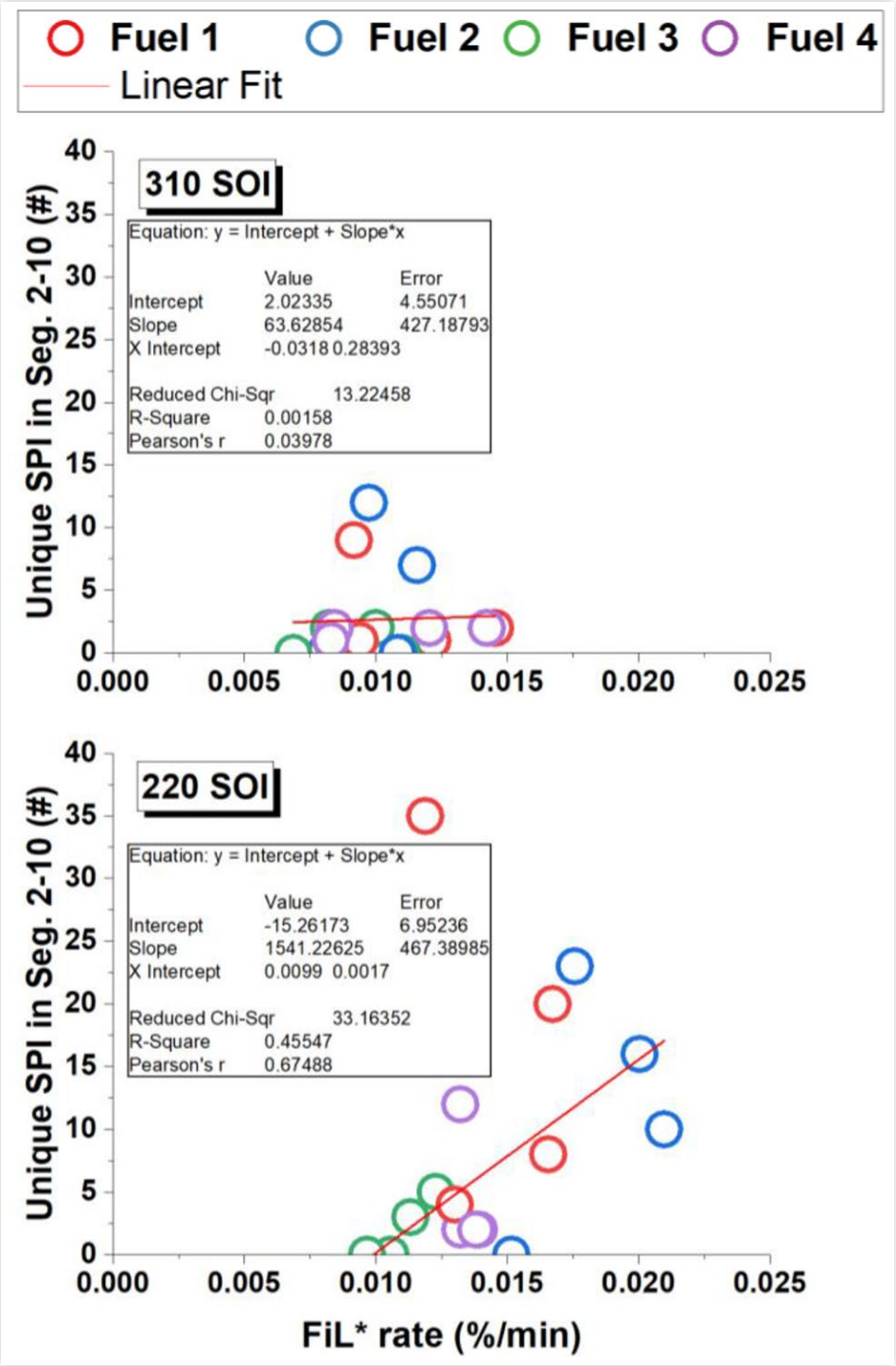

forms the liquid layer. SPI rates were found to be well correlated with *FiL** when fuel was impinged on the cylinder liner, suggesting that there was a physical relation and dependency of SPI on fuel distillation temperature, engine surface temperature, and fuel—liner impingement.

- PMI and *FiL** were found to be notionally related, but deviations existed with fuels that had higher final boiling points combined with high volatility below T50 (i.e., E25/T5 fuel), suggesting that there was a physical relation and dependency of *FiL** that was not well captured by PMI.

This Phase 1 work for the AVFL-33 project highlights physical processes demonstrated to affect SPI through direct measurements combined with theory. The results demonstrate

FIGURE 14 Fuel PMI as a function of *FiL** for 310°CA SOI timing (top row), 220°CA SOI timing (bottom row), 90°C coolant temperature (left column), and 70°C coolant temperature (right column). Data markers are color-coded by fuel; boost levels are not delinated.

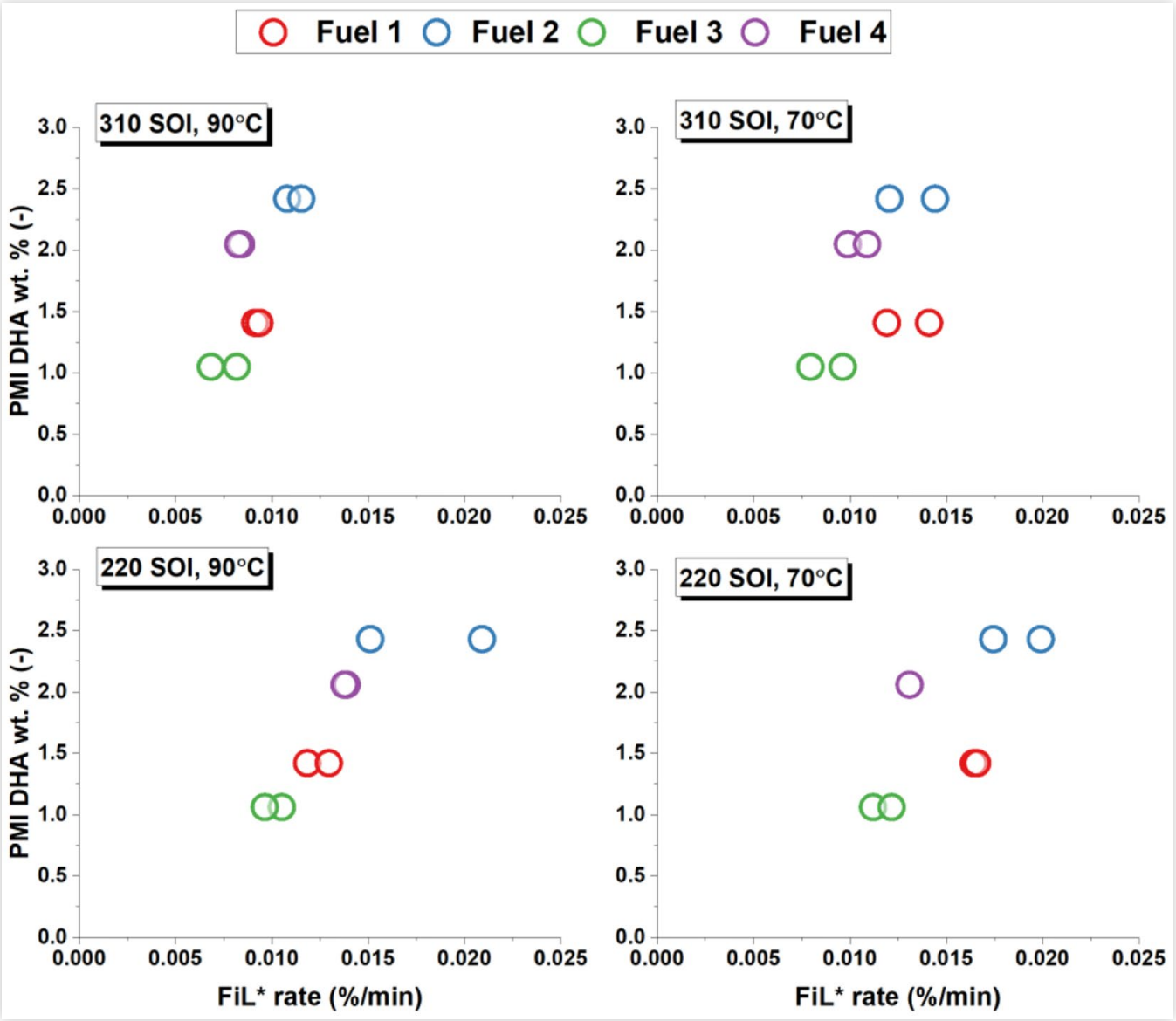

conditions that generate elevated SPI rates and serve as a foundation for future fuel property investigations of SPI at SPI-prone conditions (i.e., using an approach similar to the present work but with down-selected operating conditions and a broader fuel matrix).

Legal Notice

References

1. Willand, J., Daniel, M., Montefrancesco, E. et al., "Limits on Downsizing in Spark Ignition Engines Due to Pre-Ignition," *MTZ Worldw* 70 (2009): 56-61, https://doi.org/10.1007/BF03226955.
2. Costanzo, V., Yu, X., Chapman, E., and Davis, R., "Fuel Effects on the Propensity to Establish Propagating Flames at SPI-Relevant Engine Conditions," SAE Technical Paper 2021-01-0488 (2021), https://doi.org/10.4271/2021-01-0488.
3. Yokoo, N. et al. "The Effect of Fuel Compositions on Pre-ignition under High Temperature and High Pressure Condition by Imitating Boost Engine," JSAE Technical Paper 57-20105557, 2010.
4. Gunther, M. et al., "Enthalpy-Based Approach to Quantifying and Preventing Pre-Ignition," MTZ 04/2011 Vol. 72, 2011.
5. Zahdeh, A., Rothenberger, P., Nguyen, W., Anbarasu, M. et al., "Fundamental Approach to Investigate Pre-Ignition in Boosted SI Engines," *SAE Int. J. Engines* 4, no. 1 (2011): 246-273, https://doi.org/10.4271/2011-01-0340.
6. Jatana, G.S., Splitter, D.A., Kaul, B., and Szybist, J.P., "Fuel Property Effects on Low-Speed Pre-Ignition," *Fuel* 230 (2018): 474-482.
7. Splitter, D., Kaul, B., Szybist, J., and Jatana, G., "Engine Operating Conditions and Fuel Properties on Pre-Spark Heat Release and SPI Promotion in SI Engines," *SAE Int. J. Engines* 10, no. 3 (2017): 1036-1050, https://doi.org/10.4271/2017-01-0688.
8. Kalghatgi, G.T. and Bradley, D., "Pre-Ignition and 'Super-Knock' in Turbo-Charged Spark-Ignition Engines," *International Journal of Engine Research* 13, no. 4 (2012): 399-414.
9. Splitter, D., Kaul, B., Szybist, J., Speed, L. et al., "Fuel-Lubricant Interactions on the Propensity for Stochastic Pre-Ignition," SAE Technical Paper 2019-24-0103 (2019, 2019), https://doi.org/10.4271/2019-24-0103.
10. Chapman, E. and Costanzo, V., "A Literature Review of Abnormal Ignition by Fuel and Lubricant Derivatives," *SAE Int. J. Engines* 9, no. 1 (2016): 107-142, https://doi.org/10.4271/2015-01-1869.
11. Takeuchi, K., Fujimoto, K., Hirano, S., and Yamashita, M., "Investigation of Engine Oil Effect on Abnormal Combustion in Turbocharged Direct Injection - Spark Ignition Engines," *SAE Int. J. Fuels Lubr.* 5, no. 3 (2012): 1017-1024, https://doi.org/10.4271/2012-01-1615.
12. Gohl, M., Brandt, S., Wittler, M., Budde, M. et al., "Influence of the Mixture Formation on the Lubrication Oil Emission of Combustion Engines," *SAE Int. J. Fuels Lubr.* 3(1):733-744, 2010, https://doi.org/10.4271/2010-01-1275.
13. Takeuchi, K., Fujimoto, K., Hirano, S., and Yamashita, M., "Investigation of Engine Oil Effect on Abnormal Combustion in Turbocharged Direct Injection-Spark Ignition Engines," *SAE Int. J. Fuels Lubr.* 5, no. 3 (2012): 1017-1024, https://doi.org/10.4271/2012-01-1615.
14. Haenel, P., Seyfried, P., Kleeberg, H., and Tomazic, D., "Systematic Approach to Analyze and Characterize PreIgnition Events in Turbocharged Direct-Injected Gasoline Engines," SAE Technical Paper 2011-01-0343 (2011), https://doi.org/10.4271/2011-01-0343.
15. Kalghatgi, G., Algunaibet, I., and Morganti, K., "On Knock Intensity and Superknock in SI Engines," *SAE Int. J. Engines* 10, no. 3 (2017): 1051-1063, https://doi.org/10.4271/2017-01-0689.
16. Fletcher, K.A., Dingwell, L., Yang, K., Lam, W.Y. et al., "Engine Oil Additive Impacts on Low Speed Pre-Ignition," *SAE Int. J. Fuels Lubr.* 9, no. 3 (2016): 612-620, https://doi.org/10.4271/2016-01-2277.
17. Ritchie, A., Boese, D., and Young, A.W., "Controlling Low-Speed Pre-Ignition in Modern Automotive Equipment Part 3: Identification of Key Additive Component Types and Other Lubricant Composition Effects on Low-Speed Pre-Ignition," *SAE Int. J. Engines* 9, no. 2 (2016): 832-840.
18. Kocsis, M.C., Briggs, T., and Anderson, G., "The Impact of Lubricant Volatility, Viscosity and Detergent Chemistry on Low Speed Pre-Ignition Behavior," *SAE Int. J. Engines* 10, no. 3 (2017): 1019-1035.
19. Szybist, J.P., Busch, S., McCormick, R.L., Pihl, J.A. et al., "What Fuel Properties Enable Higher Thermal Efficiency in Spark-Ignited Engines?" *Progress in Energy and Combustion Science* 82 (2021): 100876, https://doi.org/10.1016/j.pecs.2020.100876.
20. Kar, A., Huisjen, A., Aradi, A., Reitz, J. et al., "Assessing the Impact of Lubricant and Fuel Composition on LSPI and Emissions in a Turbocharged Gasoline Direct Injection Engine," *SAE Int. J. Advances & Curr. Prac. in Mobility* 2, no. 5 (2020): 2568-2580, https://doi.org/10.4271/2020-01-0610.
21. Ohtomo, M. et al., "Pre-Ignition of Gasoline-Air Mixture Triggered by a Lubricant Oil Droplet," *SAE Int. J. Fuels Lubr.* 7, no. 3 (2014): 673-682.
22. Mayer, M., Hofmann, P., Geringer, B., Williams, J. et al., "Influence of Different Oil Properties on Low-Speed Pre-Ignition in Turbocharged Direct Injection Spark Ignition Engines," SAE Technical Paper 2016-01-0718 (2016), https://doi.org/10.4271/2016-01-0718.
23. Aikawa, K., Sakurai, T., and Jetter, J.J., "Development of a Predictive Model for Gasoline Vehicle Particulate Matter Emissions," *SAE Int. J. Fuels Lubr.* 3, no. 2 (2010): 610-622, https://doi.org/10.4271/2010-01-2115.
24. Boronat Colomer, V., Splitter, D., Neupane, S., and Partridge, W., "Particle Matter Index and Fuel Wall-Wetting Relations on Stochastic Pre-Ignition," *SAE Int. J. Adv. & Curr. Prac. in Mobility* 4, no. 2 (2022): 636-648, https://doi.org/10.4271/2021-01-1163.
25. Ohtomo, M. et al., "Pre-Ignition of Gasoline-Air Mixture Triggered by a Lubricant Oil Droplet," *SAE Int. J. Fuels Lubr.* 7, no. 3 (2014): 673-682.
26. Wang, Z. et al., "Analysis of Pre-Ignition to Super-Knock: Hotspot-Induced Deflagration to Detonation," *Fuel* 144 (2015): 222-227.

27. Kassai, M., Hashimoto, H., Shiraishi, T., Teraji, A. et al., "Mechanism Analysis on LSPI Occurrence in Boosted S. I. Engines," SAE Technical Paper 2015-01-1867 (2015), https://doi.org/10.4271/2015-01-1867.
28. Watson, S.A.G., "Lubricant-Derived Ash-In-Engine Sources and Opportunities for Reduction," PhD thesis Massachusetts Institute of Technology, 2010.
29. Saville, S.B., Gainey, F.D., Cupples, S.D., Fox, M.F. et al., "A Study of Lubricant Condition in the Piston Ring Zone of Single-Cylinder Diesel Engines under Typical Operating Conditions," SAE Technical Paper 881586 (1988), https://doi.org/10.4271/881586.
30. Nattrass, S.R., Thompson, D.M., and McCann, H., "First In-Situ Measurement of Lubricant Degradation in the Ring Pack of a Running Engine," SAE Technical Paper 942026 (1994), https://doi.org/10.4271/942026.
31. Frottier, V., Heywood, J.B., and Hochgreb, S., "Measurement of Gasoline Absorption into Engine Lubricating Oil," SAE Technical Paper 961229 (1996), https://doi.org/10.4271/961229.
32. Splitter, D., Burrows, B., and Lewis, S., "Direct Measurement and Chemical Speciation of Top Ring Zone Liquid during Engine Operation," SAE Technical Paper 2015-01-0741 (2015), https://doi.org/10.4271/2015-01-0741.
33. Kim, J.S., Min, B.S., Lee, D.S., Oh, D.Y. et al., "The Characteristics of Carbon Deposit Formation in Piston Top Ring Groove of Gasoline and Diesel Engine," SAE Technical Paper 980526 (1998, 1998), https://doi.org/10.4271/980526.
34. Lee, P.M., Priest, M., Stark, M.S., Wilkinson, J.J. et al., "Extraction and Tribological Investigation of Top Piston Ring Zone Oil from a Gasoline Engine," *Proceedings of the Institution of Mechanical Engineers, Part J: Journal of Engineering Tribology* 220, no. 3 (2006): 171-180.
35. Watanabe, I., Kawai, T., Yonezawa, K., and Ogawa, T., "The New Toyota 2.0-Liter Inline 4-Cylinder ESTEC D-4ST Engine - Turbocharged Direct Injection Gasoline Engine," in *23rd Aachen Colloquium Automobile and Engine Technology*, Aachen, 2014.
36. Dahnz, C., Han, K., Spicher, U., Magar, M. et al., "Investigations on Pre-Ignition in Highly Supercharged SI Engines," *SAE Int. J. Engines* 3, no. 1 (2010): 214-224, https://doi.org/10.4271/2010-01-0355.
37. Splitter, D., Boronat Colomer, V., Neupane, S., Dal Forno Chuahy, F. et al., "In Situ Laser Induced Florescence Measurements of Fuel Dilution from Low Load to Stochastic Pre Ignition Prone Conditions," SAE Technical Paper 2021-01-0489 (2021), https://doi.org/10.4271/2021-01-0489.
38. Splitter, D., Boronat Colomer, V., Neupane, S., and Partridge, W. Jr., *Fuel Properties Effects on Wall-Wetting and Fuel-In-Lube Dilution under Stochastic Pre Ignition Prone Conditions* (Oak Ridge, TN: Oak Ridge National Lab.(ORNL), 2021)
39. Neupane, S., Boronat, V., Splitter, D., and Partridge, W.P., "An improved Method for Determining Transient Fuel Dilution of Oil in an Internal-Combustion Engine Using Laser-Induced Florescence and Multivariate Least Square Calibration," *Applied Spectroscopy* 75, no. 10 (2021): 1237-1250.
40. Parks, J., Partridge, B., and Whitacre, S., "Rapid In Situ Measurement of Fuel Dilution of Oil in a Diesel Engine Using Laser-Induced Fluorescence Spectroscopy," SAE Technical Paper 2007-01-4108 (2007), https://doi.org/10.4271/2007-01-4108.
41. Szybist, J.P., Youngquist, A.D., Barone, T.L., Storey, J.M. et al., "Ethanol Blends and Engine Operating Strategy Effects on Light-Duty Spark-Ignition Engine Particle Emissions," *Energy & Fuels*. (2011).
42. Neupane, S. et al., *Measurement of Engine-Oil Fuel Dilution Using Laser Induced Florescence Spectroscopy* (Oak Ridge, TN: Oak Ridge National Lab.(ORNL), 2020)
43. Splitter, D.A. and Szybist, J.P., "Experimental Investigation of Spark-Ignited Combustion with High-Octane Biofuels and EGR. 1. Engine Load Range and Downsize Downspeed Opportunity," *Energy & Fuels* 28, no. 2 (2014): 1418-1431.
44. Cavina, N., Siviero, C., and Suglia, R., "Residual Gas Fraction Estimation: Application to a GDI Engine with Variable Timing and EGR," SAE Technical Paper 2004-01-2943 (2004), https://doi.org/10.4271/2004-01-2943.
45. Woschni, G., "A Universally Applicable Equation for the Instantaneous Heat Transfer Coefficient in the Internal Combustion Engine," SAE Technical Paper 670931 (1967), https://doi.org/10.4271/670931.
46. Gatowski, J.A., Balles, E.N., Chun, K.M., Nelson, F.E. et al., "Heat Release Analysis of Engine Pressure Data," SAE Technical Paper 841359 (1984), https://doi.org/10.4271/841359.
47. Tunestål, P., "TDC Offset Estimation from Motored Cylinder Pressure Data Based on Heat Release Shaping," *Oil & Gas Science and Technology–Revue d'IFP Energies Nouvelles* 66, no. 4 (2011): 705-716.
48. Mansfield, A.B., Chapman, E., and Briscoe, K., "Impact of Fuel Octane Rating and Aromatic Content on Stochastic Pre-Ignition," SAE Technical Paper 2016-01-0721 (2016), https://doi.org/10.4271/2016-01-0721.
49. Hwang, J., Weiss, L., Karathanassis, I.K., Koukouvinis, P. et al., "Spatio-Temporal Identification of Plume Dynamics by 3D Computed Tomography using Engine Combustion Network Spray G Injector and Various Fuels," *Fuel* 280 (2020): 118359.
50. Mills, Z.G., Finney, C.E., Haynes, J.A., Trofimov, A.A. et al., "Impact of Materials Properties on Higher-Temperature Engine Operation," SAE Technical Paper 2021-01-1142 (2021), https://doi.org/10.4271/2021-01-1142.

Contact Information

Derek Splitter
splitterda@ornl.gov

Acknowledgments

This research was supported by the Coordinating Research Council under CRC Project AVFL-33 under contract with Oak Ridge National Laboratory as a Strategic Partnership Project.

The Coordinating Research Council, Inc. (CRC) is a non-profit corporation supported by the petroleum and automotive equipment industries. CRC operates through the committees

made up of technical experts from industry and government who voluntarily participate. The four main areas of research within CRC are: air pollution (atmospheric and engineering studies); aviation fuels, lubricants, and equipment performance; heavy-duty vehicle fuels, lubricants, and equipment performance (e.g., diesel trucks); and light-duty vehicle fuels, lubricants, and equipment performance (e.g., passenger cars). CRC's function is to provide the mechanism for joint research conducted by the two industries that will help in determining the optimum combination of petroleum products and automotive equipment. CRC's work is limited to research that is mutually beneficial to the two industries involved. The final results of the research conducted by, or under the auspices of, CRC are available to the public.

Abbreviations

°C - degrees Celsius

°CA - degrees crank angle

°CA bTDC$_f$ - crank angle degrees before top dead center firing

ASTM - American Society for Testing and Materials

bar - bar pressure unit

CA02 - crank angle of 2 percent mass fraction burned

CA50 - crank angle of 50 percent mass fraction burned

E0 - 0% ethanol by volume

E25 - 25% ethanol by volume

E25/T5 - 25% ethanol by volume and 5% tetralin by volume

FiL - fuel in lube

FiL* - Fuel in lube modified

gal. - gallon

GDI - gasoline direct injection

hp - horsepower

IMEP$_g$ - gross indicating mean effective pressure

in. - inches

kPa - kilopascal

l - liters

mm - millimeter

MON - Motor Octane Number

nm - nanometers

PMI - Particulate matter index

ppm - parts per million

RON - Research Octane Number

rpm - revolutions per minute

S - Fuel sensitivity

SCE - single-cylinder engine

SI - spark ignition

SOI - start of injection

SPI - stochastic preignition

T5 - 5% tetralin by volume

T50 - 50 percent mass faction boiled

TDC - Top dead center

TRZ - top ring zone

vol. - Volume

wt. - weight

Appendix A: Baseline Results

A baseline condition was operated after every fourth test and repeated with multiple replications (either two or three) when new engine installations and break-in procedures were complete. Three engines were used in this study, and engines were replaced because of engine wear over the total study duration.

The baseline condition was a full 10 segment experiment using the same operating schedule as that presented in Figure 3, operated at 185 kPa intake pressure, 90°C coolant and oil temperature, and 280 bTDC$_f$ SOI timing (unique to the other conditions in this study but a similar SOI timing as used in the production engine). All baselines were operated with Tier II certification grade E0 Haltermann HF0437 fuel, and the

TABLE 6 Baseline fuel, Haltermann HF0437 Tier II EEE fuel properties.

	Haltermann HF0437 EEE
RON (–) (ASTM D2699)	97.4
MON (–) (ASTM D2700)	89.0
S (–) (RON – MON)	8.4
IBP (°F) (ASTM D86)	86
T5 (°F) (ASTM D86)	109
T10 (°F) (ASTM D86)	123
T20 (°F) (ASTM D86)	141
T30 (°F) (ASTM D86)	162
T40 (°F) (ASTM D86)	189
T50 (°F) (ASTM D86)	215
T60 (°F) (ASTM D86)	230
T70 (°F) (ASTM D86)	240
T80 (°F) (ASTM D86)	256
T90 (°F) (ASTM D86)	312
T95 (°F) (ASTM D86)	339
FBP (°F) (ASTM D86)	400
Residual (vol. %) (ASTM D86)	0.8
Carbon (wt. %) (ASTM D5291)	86.67
Hydrogen (wt. %) (ASTM D5291)	13.33
Oxygen (wt. %) (ASTM D4815)	0
Net heating value (MJ/kg) (ASTM D240)	43.192
Density (g/ml @15.56°C) (ASTM D4052)	59.2
Specific gravity (@15.56°C) (ASTM D4052)	0.742

FIGURE 15 SPI response of the baseline condition plotted as an average SPI event per 20,000 cycle segments as a function of engine life (test number)

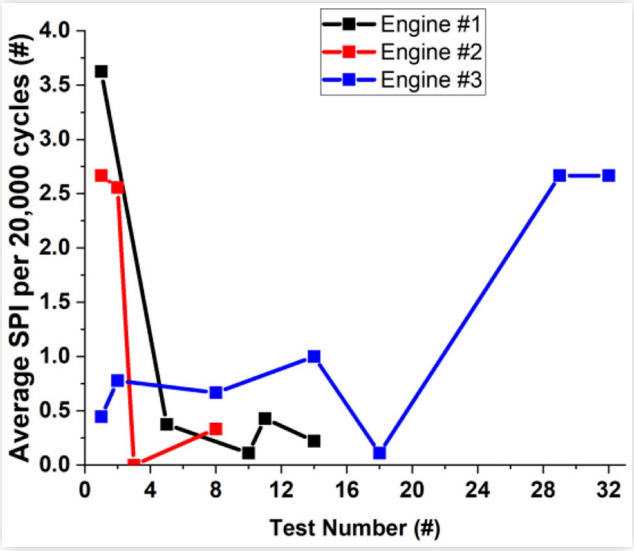

fuel properties are described in Table 6. As noted in the table, the fuel properties of the control fuel are very similar to the base fuel used in the main study.

The SPI response of the engines at the baseline condition is plotted in Figure 15. The data are presented as an average SPI events per segment (i.e., numerical average of SPI on a per-segment basis by dividing the total unique SPI measured for a given test by the number of segments in that test) as a function of test number (number of experiments on a given engine). Results demonstrate that engines 1 and 2 show a rapid decrease in SPI response as a function of engine age (test number), whereas engine 3 shows an inverse trend where at longer engine age the SPI response increased. Based on the results, where the SPI response was similar for all engines in the after-break-in period (except engine 3 at near the end of life) no corrections to SPI response with respect to engine age were made in this study.

e-ISSN 2641-9645